PERGAMON

International Journal of Heat and Mass Transfer 42 (1999) 1097–1110

International Journal of HEAT and MASS TRANSFER

The effect of air bubbles on the diffusion-controlled solidification of water and aqueous solutions of ammonium chloride

Marcus V. A. Bianchi*, Raymond Viskanta

Heat Transfer Laboratory, School of Mechanical Engineering, Purdue University, West Lafayette, IN 47097-1288, U.S.A.

Received 4 November 1997; in final form 31 March 1998

Abstract

Gas pores appear during solidification when the gas concentration in the liquid is higher than the gas solubility at a certain location. Since the thermal conductivity of the gas can be orders of magnitude lower than that of the solid phases, the effective thermal conductivity of the porous solid may be lower when gas bubbles are present. In this study, experiments have been carried out to determine the effect of air bubbles on the process of solidification and solid formation. Water and ammonium chloride solutions have been solidified under diffusion controlled conditions and the temperature distributions as well as the interface positions have been measured during the experiments. The amount of dissolved air in the liquid was determined by controlling the pressure of the test cell, which was placed under a bell jar. The results of the experiments show that nucleation of air bubbles at the interface does not significantly affect the effective thermal conductivity of the solid. The results are supported using microscopic experimental observations of the bubble nucleation and growth.

Nomenclature

C salt concentration
H height of the test cell
T_C cold temperature
T_H hot temperature
t time
x length measured from the cold heat exchanger.

Greek symbols

ξ dimensionless interface position, x/H
θ dimensionless temperature $(T-T_C)/(T_H-T_C)$.

Subscript

i initial condition.

1. Introduction

Solidification is an important phenomenon occurring in a variety of processes in diverse fields ranging from metals casting to preservation of biological materials. In metallurgy, solidification is often the beginning of any metal production and occurs in such processes as die casting and continuous casting, welding, soldering, and metal coating. In particular, casting is a very economic method of forming a component if the melting point of the metal is not too high. It is possible to cast metal products economically from alloys of melting points as high as 1933 K (Ti) [1].

Solidification within rectangular enclosures is of considerable theoretical and practical interest in many applications, ranging from freezing of biological materials to solidification of metals. Examples of important processes are die casting [1], latent heat storage [2], freezing and preservation of blood and tissues [3], and numerous others.

Studies involving the freezing of binary alloys from below have been conducted in rectangular enclosures in which during the solidification process the lighter con-

* Corresponding author. Present address: PROMEC-UFRGS, Caixa Postal 9566, Porto Alegre, RS 90441-970, Brazil. Tel.: +55 51 316 3931; fax: +55 51 316 3355; e-mail: marcus_bianchi@yahoo.com

0017–9310/98 $19.00
PII: S0017–9310(98)00133–1

stituent is rejected to the liquid phase [4–10]. In these situations, double diffusive convection is present due to the density differences induced by thermal and solutal gradients.

Gas voids and porosity are caused by the evolution and entrapment of gas during the solidification of metals. This gas may result from several sources: (1) a decrease in solubility upon cooling from the liquid state; (2) reaction of metallic oxides with carbon to form CO and CO_2; and (3) the reaction of liquid metal with moisture in green sand molds [11]. The primary effects of gas holes and porosity are that they reduce the load carrying capacity of the member in which they occur and act as stress concentrators [11].

The study of the effects of gases on the solidification of metals began over 150 years ago, but the subject started to receive more attention in the early 1900s [12]. Keeping combustion gases away from the melt and allowing the metal to freeze in the pot, then remelting it as fast as possible, were adapted as solutions to minimize porosity in aluminum. Even so, the rejections were high and 'gas in aluminum' was even then recognized as a problem [12].

Wilcox and Kuo [13] theoretically studied the gas bubble nucleation during the crystallization of a multicomponent gas solution. They found that the tendency to form gas bubbles increases with increasing growth rate, decreasing stirring, increasing ambient gas-pressure, and decreasing height of liquid over crystal. It was also observed that, although homogeneous nucleation of bubbles is possible it is most likely that heterogeneous nucleation on the crystal surface is the main mechanism for bubble formation.

The development of blowholes during the solidification of solutions of carbon dioxide in water were experimentally studied by Vasconcellos and Beech [14]. A test cell was designed and the experiments were conducted under different pressure conditions. It was concluded that the form of blowholes associated with the planar ice/water interface may be explained in terms of the solute profile, even though the authors used a steady state solution of the solute redistribution.

Void formation in unidirectional solidification of cyclohexane was experimentally studied for both gassed and degassed liquid [15]. Blowholes were observed when gassed liquids were solidified from above and from below. Sulfredge et al. [16] performed experiments to understand the void formation during the solidification of cyclohexane and 1,4-butanediol ($C_4H_{10}O_2$). The liquid was degassed before solidification by vacuum and proved to be an important factor in the experiments performed.

Bianchi and Viskanta [17] have studied the evolution of gas species during solidification prior to bubble nucleation. The authors have found that the build up of gas species in the liquid at the interface depends on the solidification rate. For a constant solidification rate bubbles eventually nucleate because the concentration at the interface increases monotonically during solidification.

Song [10] has noted some discrepancies between the numerical predictions and experimental observations during the solidification of a 10 wt% ammonium chloride solution from below. One of the possible reasons given for the difference was the lower thermal conductivity of the air bubbles that nucleated in the interdendritic liquid.

The presence of gas bubbles may decrease the effective thermal conductivity of the solid, decreasing the solidification rate. The effective thermal conductivity of ice with air bubbles grown from water saturated with air at 1 atm, 0°C, may vary between 27% and 97% of the thermal conductivity of pure ice, calculated using the series and parallel models, respectively. No previous work dealing with this issue has been identified in the literature. An experimental study of diffusion-controlled (i.e. in the absence of advective flows) solidification of water and water-ammonium chloride solutions with a rectangular enclosure was conducted and is described in the paper. The reason for choosing the diffusion controlled solidifications is to avoid the effect of buoyancy driven flows on the solid evolution. In the absence of fluid flow, the observed physical phenomena is not as exciting, and little research attention has been given to diffusion-controlled solidification. The motivation for such an experimental study is to observe the influence of gas evolution and of the initial salt concentration (for binary solutions) on the solid formation during the phase change process, including the effect on the effective thermal conductivity of the completely solidified region and of the mushy zone (for binary solutions).

2. Experiments

2.1 Description of apparatus

An apparatus has been designed and constructed to allow for the fundamental study of diffusion-controlled undirectional solidification in a rectangular cavity. The effects of initial concentration, initial temperature, and initial gas content in the liquid can be observed and studied. Additional details of the experimental apparatus can be found elsewhere [18].

A schematic of the experimental apparatus with every component is shown in Fig. 1. The test apparatus is comprised of the following components: (1) an enclosed freezing chamber with two heat exchangers (top and bottom); (2) a bell jar vacuum system to control the initial dissolved air concentration in the liquid; (3) temperature measurement instrumentation; (4) a recirculating pump and recirculating lines for the PCM; (5) three constant temperature baths; and (6) instrumentation for tracking the interface position during solidification. The descriptions of the major test cell components are provided below.

A rectangular test cavity is filled with water or water–

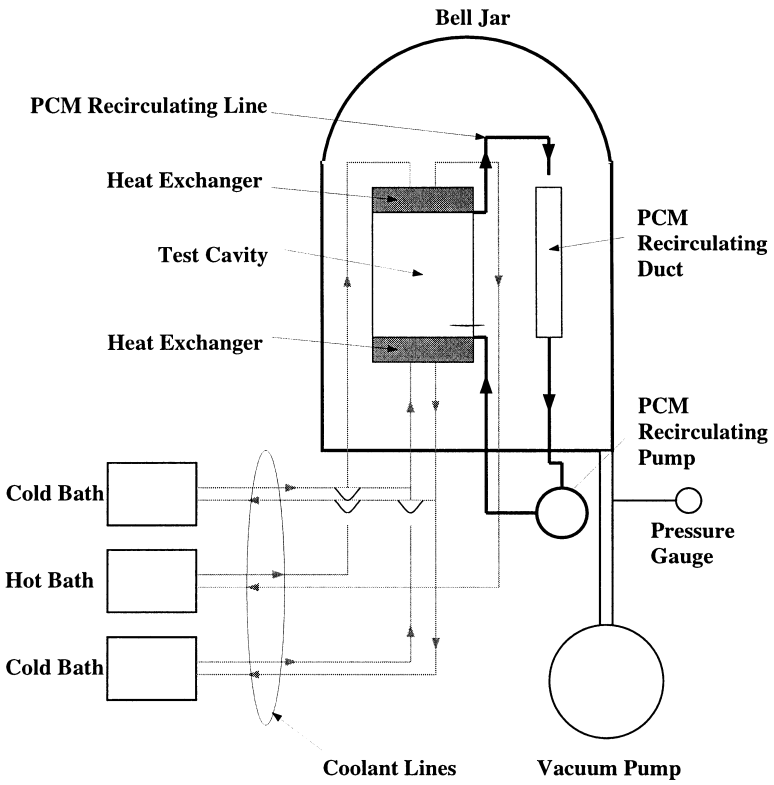

Fig. 1. Schematic of the macroscopic experimental apparatus.

ammonium chloride solutions of hypoeutectic concentration, and the horizontal walls are heated and cooled by imposing uniform temperatures, while the two pairs of the connecting vertical walls are thermally insulated. Solidification occurs on the cold horizontal wall. The vertical walls are made of transparent material (Plexiglas) to observe the interface evolution and motion. Several factors are important for the design of the test cell: (1) visual and mechanical access to the test cavity; (2) short duration of the experimental runs; (3) instrumentation access without significantly affecting the physical phenomena; (4) minimum heat gains from the environment; and (5) means to freeze from both the top and the bottom of the cavity.

Solidification of air saturated water or NH_4Cl–water solution takes place within the rectangular cross-section test cavity having the dimensions of 127 mm in height, 102 mm in width, and of 25.4 mm in depth. Since quantitative measurement of the interface progression is of interest, the connecting walls (front, back and side walls) are all made of 12 mm thick Plexiglas plates. The connecting walls are placed between the two heat exchangers with sealing provided by an o-ring whose seating is milled in the Plexiglas walls at the top and bottom surfaces. Two access holes are placed at the top and side walls for two reasons: (1) to recirculate the phase change material (PCM) before and after the experiments. This is particularly convenient to achieve uniform initial temperature and also to fill and empty the cavity and the system; and (2) to maintain a constant volume of the density difference between the solid and liquid phases during phase transformation, contraction or expansion may occur during freezing and it requires a net inflow or outflow of liquid.

The top and bottom walls of the test cell, which served as the hot and cold sinks, are made of 6 mm thick copper plates. Ethyl alcohol (200 proof) is circulated from the constant temperature baths (2 NESLAB ULT-80DD) to the cold heat exchanger, while a mixture of water (80%) and ethyl alcohol (20%) from the other constant temperature bath (HAAKE A82 for the hot heat exchanger) circulated through the channels milled in the copper and the 4 mm stainless steel back plates. Each heat exchanger, which is an assembly of a milled copper plate and a stainless steel back plate, had one coolant passage which extended along the entire length of the copper plate. Three thermocouple probes are placed in the copper plate near the liquid (0.5 mm separation) to check isothermal-

ity. The thermocouple junctions are set in the milled grooves by a high conductivity epoxy and are routed through the copper plate up to the end of the grooves.

To measure the temperature of the PCM within the cavity, type-T thermo-couple probes are mounted on the back wall. Stainless steel straight thread o-ring male connectors (Swagelock-100-1-2ST) are used to mount the probes through the back wall. This design is more appropriate than placing a vertical rake because it minimizes the influence of the temperature measurements on the solidifying system. Since heat conduction is the controlling mechanism for solidification, placing a rake parallel to the heat flux may affect the measured temperatures due to the heat conduction through the rake. The location of each thermocouple relative to the cold heat exchanger is 1, 16, 32, 48, and 64 mm. The connecting walls could be rotated 180°C so the thermocouple probes could be placed close to the top or the bottom heat exchanger. Since solutions of NH_4Cl in water are very corrosive, both heat exchangers are coated with a thin layer of black paint.

To minimize heat gain by the freezing chamber, the connecting walls are insulated with a removable 25 mm thick polystyrene insulation. A narrow slot (10 mm) is cut on the insulating plate of the front wall in order to provide visual access to the freezing chamber.

The entire test assembly, including the test cell, heat exchangers and the insulation, is placed over a 25 mm thick G-7 plate, which with the bell jar forms the vacuum chamber. This serves two purposes: (1) to create the vacuum for the degasification of the liquid within the enclosure; and (2) to minimize the heat gain from the surroundings. A vacuum pump and a pressure gauge complete the experimental apparatus.

2.2. Interface locations

The solid–liquid interface (for water experiments) and the solidus and liquidus fronts (for binary mixtures) are observed through the Plexiglas freezing chamber back and front walls. A scale attached to the front wall is used to measure the interface position relative either to the top (for water experiments) or the bottom (for binary mixtures) of the freezing cavity during the course of the experiments. The accuracy of this measurement is ± 1 mm. Visual observations through the side walls reveal that the interfaces are in fact planar, with a slight sloping (less than 1 mm vertical displacement) close to the vertical walls. This is due to the heat gain from the ambient surroundings, and this effect is much larger (over 3 mm vertical displacement near the Plexiglas wall) in the absence of insulation around the cavity, where solidification is taking place.

The position of the interfaces (solid–liquid for water, and liquidus and solidus for salt solutions) is tracked using a CCD camera (Sony model AVC-D7) connected to a VCR. The progression of each experiment is recorded on a video-tape.

2.3. Temperatures

All temperatures are measured with copper–constantan (Type-T) thermocouples. The probes used inside the test cavity are made by Omega (Omega subminiature thermocouple probes—quick disconnect style—TMQSS-062G-2), while the seven other thermocouple junctions (six for the two heat exchangers and one for the ambient air) are manufactured from 0.127 mm wire.

Using a thermal bath with temperatures ranging from -40°C to 20°C, relative accuracy of all the thermocouples used in this study is determined to be less than ± 0.03°C. To determine the absolute accuracy of the thermocouples a known temperature standard must exist. Ice was made from deionized water and a mixture of deionized water and crushed ice was used as a standard. Placing the thermocouples in this mixture, the measured temperatures were within -0.06–0.01°C.

As mentioned before, the uniformity of the surface temperature of the two heat exchangers is monitored with three thermocouples mounted at the centerline of the copper plates. During the experiments, the temperatures measured by the three thermocouples located in the copper plates were within the uncertainty of the temperature measurements (± 0.1°C).

2.4. Gas concentrations and pressure

The gas solubility is a strong function of the pressure. The higher the pressure the higher the amount of gas that can dissolve in the liquid. To control the initial gas content in the melt the pressure in the bell jar is controlled by a vacuum pump. By controlling the pressure, it is also possible to remove the gas from the melt prior to solidification.

A mechanical vacuum gauge (Heise H38773) is used to monitor the pressure around the test cell and it has a 0.1 in Hg resolution. The vacuum is produced by a duo seal vacuum pump (W. M. Welch Manufacturing Company). A system of vacuum rated hoses connects the pump and the test cell with a valve in-between.

The dissolved air concentration of the phase change material had to be measured before starting each experiment. A hand-held dissolved oxygen system (YSI, Model 55) is used to measure the concentration. The probe, however, presents no compensation for measuring air content of salt solutions other than sodium chloride. Therefore, the dissolved gas concentration results presented for ammonium chloride solutions should be regarded as qualitative.

2.5. Experimental procedure

The preparation of each experiment consisted of the following steps: (1) preparation of the ammonium chlor-

ide solution of predetermined concentration (for the binary mixture experiments); (2) the assembly of the test cell with the vacuum chamber; (3) filling of the test cavity and recirculation loop with the phase change material; (4) degassing of the PCM; and (5) achievement of the uniform initial temperature throughout the test cell.

The solution of a predetermined concentration was obtained by mixing deionized water of a resistivity larger than 15 Mohm-cm with a requisite amount of research grade ammonium chloride grains (J. T. Baker, Inc.).

The test cell is filled from the Plexiglas recirculating reservoir, and the phase change material is recirculated through the pump (which is not turned on), filling the test cavity by the difference in static pressure. The filling process is accomplished carefully to avoid the entrapment of large air bubbles in the test cavity. In the case of air bubbles were trapped, the recirculating liquid (with the recirculating pump on) eventually removed the bubbles.

Degassing was achieved by simultaneously creating a vacuum and recirculating the PCM. The initial uniform temperature condition was reached by controlling the temperatures of both heat exchangers. In the absence of PCM recirculation, the process to achieve uniform low initial temperature inside the test cavity would be very slow, because it is controlled by heat diffusion. Since the initial temperature is lower than the room temperature for some experiments and due to the poor heat transfer rate, the phase change material is circulated inside the test cell using a fish tank pump (Supreme Mag-Drive model 2 250 GPH) to accelerate the cooling of the phase change material. The heat exchanger temperatures were set 2°C below the predetermined initial temperature at first and were readjusted to the desired initial temperature when all the liquid in the test cavity was 1°C below the temperature. This process took about 3 h for desired initial temperatures of −2°C when the ambient temperature is 20°C.

While the PCM is recirculating inside the test cavity to achieve uniform initial temperature, the pressure outside the cavity is lowered to degas the liquid. The degassing process starts with the PCM recirculating in the system with both heat exchangers maintained at a temperature slightly smaller than the target initial temperature. The vacuum pump is turned on and the valve is slowly opened subjecting the bell jar-plate cavity to the vacuum. As the pressure inside the cavity drops, air bubbles start to nucleate on the cavity walls and recirculating reservoir. The vacuum is increased slowly step-by-step, and during the experiments the degassing process is performed in two steps at 20.0 and 29.0 in Hg vacuum. During the 3 h that the pressure is maintained at high vacuum, the gas escapes the system through the recirculating reservoir.

When the initial temperature and initial gas concentration are reached, the data acquisition system is started in order to store the temperature data and, simultaneously, the CCD camera starts to record the progression of the experiment. Then, through a system of valves, the second constant temperature bath (connected to the cold heat exchanger) starts to recirculate very cold coolant through the heat exchanger. To ensure fast response of the system, one 0.1 horsepower booster pump (Cole Parmer L-07002-72) is installed on the discharge side of the cold temperature bath to increase the coolant flow rate.

3. Results and discussion

Solidification experiments were conducted with air saturated water at three different gas concentrations (saturated at atmospheric pressure, degassed, and supersaturated) and ammonium chloride solutions with four different concentrations (1, 6, and 10 wt%). (Additional results can be found elsewhere [18].) The amount of air dissolved in the phase change material is controlled by the pressure inside the bell jar. Table 1 summarizes the experimental conditions which are discussed in this paper.

In the notation in Table 1, the different phase change materials are noted with the capital letters W (for water)

Table 1
Summary of the macroscopic experimental conditions

Experiment	Orientation	C_i (wt%)	Pressure (atm)	Gassing (saturation)	T_H (°C)	T_C (°C)
WD	Downward	0	1	degassed (4%)	3.5	−27
WA		0	1	saturated (98%)	3.5	−27
WS		0	0.3	saturated (99%)	3.5	−27
S01D	Upward	1	1	degassed (7%)	3	−32.5
S01A		1	1	saturated (98%)	3	−32.5
S06D		6	1	degassed (5%)	1	−30
S06A		6	1	saturated (98%)	1	−30
S10D		10	1	degassed (5%)	−1	−40
S10A		10	1	saturated (96%)	−1	−40

and S (for solution). The water experiments differ from each other because of the initial dissolved air concentration in the liquid: A for saturated at atmospheric pressure, D for degassed, and S for supersaturated. For the supersaturated case, water was saturated at 1 atm and the experiment was performed at a lower pressure (0.3 atm). The salt solution experiments have a slightly different notation. First, the salt concentration is noted by the two digits following S: 01 for 1 wt%, 06 for 6 wt%, and 10 for 10 wt%. Then, the initial dissolved air concentration in the liquid is noted by either A or D.

3.1. Downward solidification of water

To assess the effect of the dissolved gas evolution during solidification separated from morphology effects, deionized water is used as the phase change material. Water reaches its maximum density at 3.98°C [19]. Therefore, to perform a diffusion-controlled solidification of water (avoiding convective effects) it is necessary to freeze it from the top and have the initial temperature lower or equal to 3.98°C. The experiments reported in this section were performed with an initial temperature of 3.5°C. The temperature distribution is one-dimensional, and the interface is planar and horizontal.

In Fig. 2 the solid–liquid interface location visually observed during Experiments WD, WA and WS is shown. The interface position is compared to assess the effect of the dissolved air on the solidification rate. The interface position for the water saturated at atmospheric pressure agrees very well with that for the dissolved water, with very little difference. It is clear from the data that the interface position is not significantly affected by the presence of gas bubbles in the ice. For saturated water at 1 atm and for degassed water, the interface position is exactly the same. This means that the presence of air bubbles does not play a role on the thermal conductivity of the solid.

The interface velocity is large only for a very brief period of time at the beginning of the experiment, but falls to about 80 μ s^{-1} after only 20 s into the process, to about 15 μm s^{-1} after 500 s, and then to 5 μ s^{-1} at the end of the experiment. Experiments were conducted using a cryomicroscope to investigate the growth of air bubbles in water on a microscopic scale [18]. For low solidification rates (less than 20 μm s^{-1}), gas bubbles grow as blowholes, i.e. long elongated cylindrical bubbles. Figure 3 shows the growth of an air blowhole during solidification of water at a rate of 10 μm s^{-1} [18]. Since during most of the experiment the interface propagation favors the growth of blow-holes, the effective thermal conductivity of the ice can be calculated assuming that

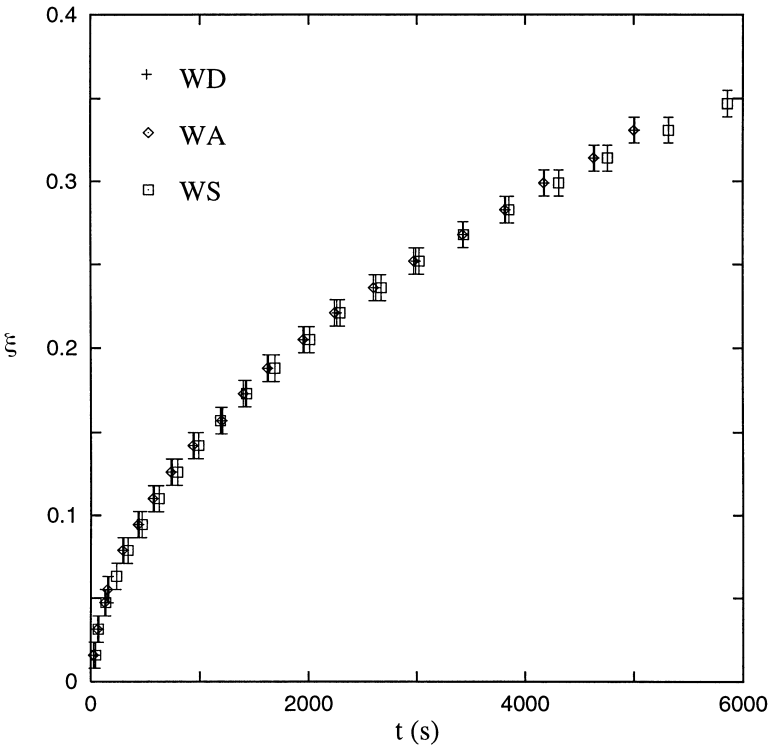

Fig. 2. Comparison of the interface location along the vertical line.

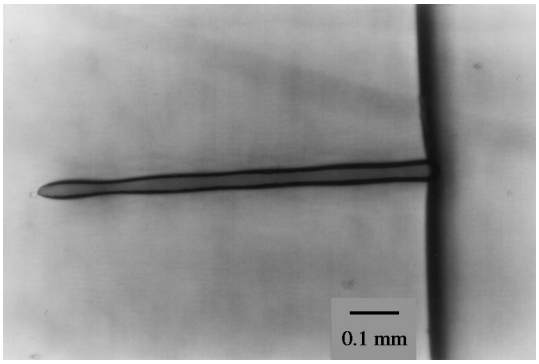

Fig. 3. Typical blowhole growing at a solidification rate of 10 μm s^{-1} [18].

the resistances in the ice and in the air are in parallel (details of thermal resistance calculations can be found elsewhere [20]), resulting in a value 97% of that of pure ice. This should not significantly affect the solidification process as it is clearly seen in Fig. 2. For the supersaturated case there is a slight difference, and the interface is retarded just towards the end of the experiment compared with the other two cases. The difference though is too small. It is within the experimental uncertainty of the measurement and can be explained by the slight heat gain from the surroundings during this experiment (WS). In order to obtain visual access to the solid, no insulation was used during experiment WS. Even thought the experiment was performed under vacuum conditions, with smaller heat gain from the ambient surroundings, some heat gain occurred and slightly affected the propagation of the interface. It is clear from these experiments that the interface position is not significantly affected by the presence of gas bubbles in the solid.

Figure 4 shows the effect of the dissolved air on the transient distribution of the dimensionless temperature. Again, for experiments WD and WA, the temperature distribution agrees very well. In the liquid region there is a small difference, due to the differences in the initial temperature of the liquid before the start of each experiment. Note that the phase change temperature can be observed at $\theta = 0.885$ Due to the different thermal diffusivities of the solid and liquid phases the slope of the curves change when the liquid solidifies. It is important to note the absence of temperature fluctuations in the liquid region, $\theta > 0.885$. Presence of oscillations would suggest undesirable buoyancy driven flow in the liquid.

Figure 5 shows the transient dimensionless tem-

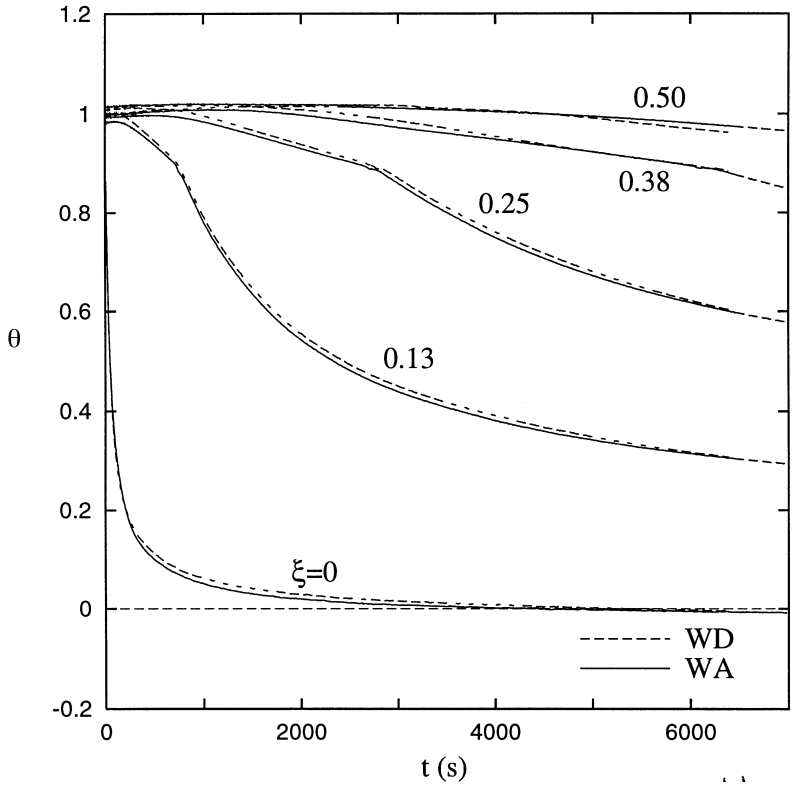

Fig. 4. Comparison of the transient temperature distributions along the vertical line (experiments WD and WA).

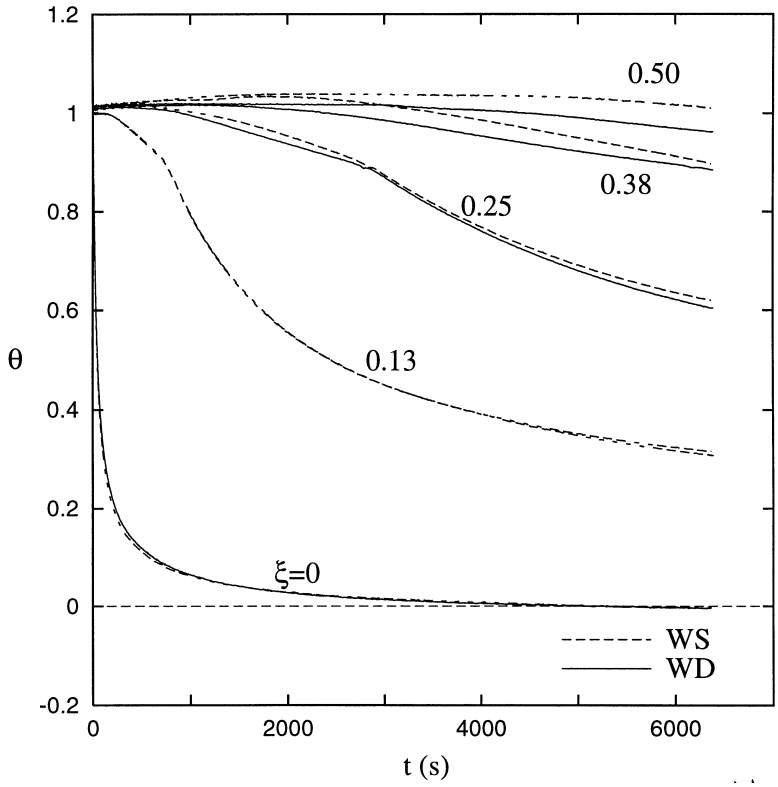

Fig. 5. Comparison of the transient temperature distributions along the vertical line (experiments WD and WS).

perature distribution for the degassed water (WD) and the supersaturated water (WS) experiments. There is excellent agreement of the temperatures in the solid region, demonstrating a negligible effect of the gas evolution on the temperature distribution, since bubbles nucleate only at the solid-liquid interface. However, there is a discrepancy in the temperature fields in the liquid region. The explanation for this discrepancy is the absence of the insulation around the test cell for the experiment with supersaturated water. Heat gain through the walls became significant as the experiment progressed, and the temperature of the liquid near the middle of the test cell was more affected than near the top heat exchanger. This was to be expected, since the liquid near the top heat exchanger solidified very quickly in comparison with the liquid away from the top heat exchanger.

Photographs of the ice structure formed in all of the experiments with water (WA, WD and WS) are shown in Fig. 6. The photographic images were recorded using the same illumination with a black background. The ice forms from the top heat exchanger (not shown in the figure) and the bottom of the photographs (darker area) represents the liquid region. The ice formed during the freezing of the saturated water (WA) is not transparent due to the presence of air bubbles. Blowholes form during the freezing process and bubbles nucleate at the solid–liquid interface. For the degassed water (WD), the ice is almost transparent, but small gas bubbles are still present in the solid; however, they cannot be observed in the Figure. This shows that the degassing process is not complete even after lowering the pressure in the bell jar. A small amount of gas will still be present in the liquid after the degassing. The ice formed from the supersaturated water is shown at the bottom. For this case (WS), the gas bubbles are large and readily visible. Large blowholes are present, and it is possible to observe them.

3.2. Upward solidification of binary alloy

Along the liquidus of the equilibrium phase diagram for the aqueous ammonium chloride solution [21], the liquid concentration increases as the temperature decreases on the hypoeutectic concentration side. Therefore, during the solidification of solutions of hypoeutectic concentrations, the interdendritic liquid near the liquidus interface is colder and richer in solute and thus denser than the initial solution. It is warmer and less rich in solute than the interdendritic liquid near the solidus interface. Thus, during the upward solidification of solutions of hypoeutectic concentrations, the buoyancy force does

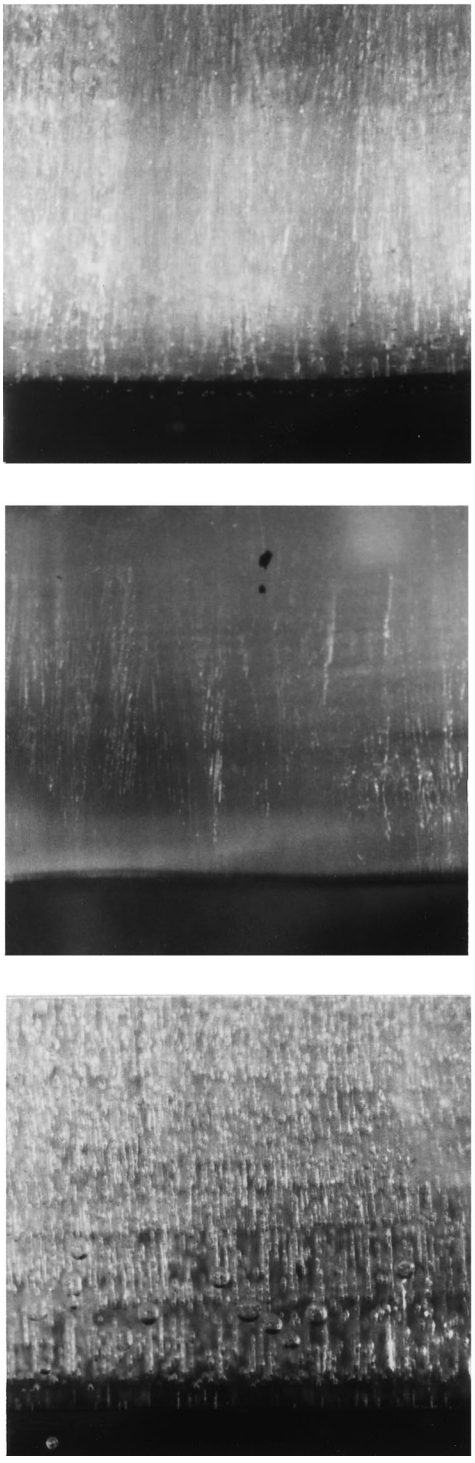

Fig. 6. Solid region for experiments (a) WA, (b) WD, and (c) WS.

not induce fluid motion, and the heat and mass transfer process are one-dimensional with the liquidus and solidus interfaces being horizontal.

3.3. Solution at 1 wt%

Since density inversion is present in water at 3.98°C, the density of low concentration salt solutions also exhibits a maximum with a temperature above the liquidus temperatures [19]. The advective flows caused by the density inversion in salt solutions have been studied for NaCl (Gebhart et al. [19] presents a comprehensive review) and $CaCO_3$ [22, 23], but no studies have been identified in the literature for solutions of NH_4Cl in water. In the most comprehensive document containing the thermophysical properties of aqueous solutions of electrolytes [24] there is no indication of the density inversion for solutions with a concentration of 2 wt%. However, the temperature of maximum density for 1, 2, and 3 wt% solutions has been reported [25]. Previous work on solidification of ammonium chloride solutions from below have avoided the density inversion, because the initial concentration of the solution was high enough. Braga and Viskanta [26] and Song [10] performed experiments with solutions of a minimum salt concentration of 5 wt% and 10 wt%, respectively.

The present experiments are performed with aqueous solutions of ammonium chloride with initial concentration as low as 1 wt%. For a concentration this low, it is expected that advective flows will be present due to the density inversion of the salt solution over a temperature range from a temperature lower than the liquidus temperature (−0.07°C) to the temperature of maximum density (2.65°C). It should be noted that it does not suffice to freeze the solution from above to avoid the density inversion effects. To obtain diffusion-controlled solidification of salt solutions, it is necessary to insure thermal and solutal stability. When freezing salt solutions from above, salt rich liquid would be rejected by the solid and would induce plume-like convection (see, for instance, the work of Magirl and Incropera [9]).

Figure 7 compares the transient dimensionless temperature distribution for the degassed (S01D) and the saturated (S01A) solution. Note that there is essentially no difference in the temperature distribution with time, even with the presence of buoyancy driven flows due to the density inversion in the solution. In the liquid region, though, the temperature oscillations are large, and it becomes more difficult to compare the temperatures for the two experiments, Note that there is an anomaly in the temperature measured by the first thermocouple in the liquid ($\xi = 0$) for the degassed solution. Either the constant temperature bath to control the temperature or the booster pump did not work properly for a short period of time. This created no major discrepancy in

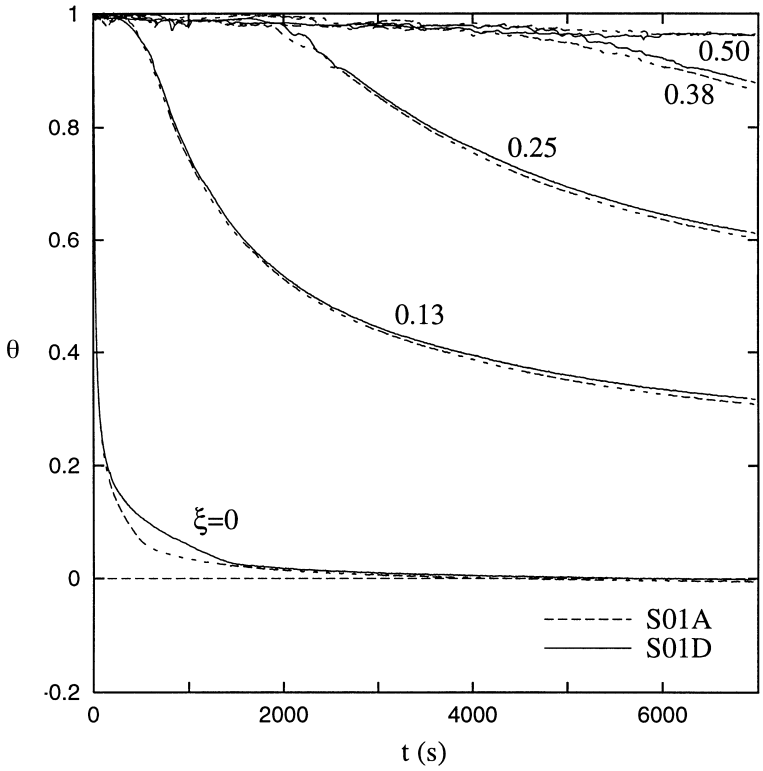

Fig. 7. Comparison of the transient dimensionless temperature (experiments S01D and S01A).

the experiments. The measured temperatures in the solid reveal an excellent agreement.

The liquidus and solidus interface positions for experiments S01D and S01A are compared in Fig. 8. The liquidus interface positions agree very well, and the differences are within the experimental uncertainty of the position measurements. The liquidus interface was clearly seen during the experiments, and it was easy to measure its position. The solidus interface, as supported by the microscopic observations, is not a sharp line and is, therefore, hard to distinguish. This is particularly the case for such a low salt concentration, since the liquid fraction when the eutectic transformation occurs is very small, and it is hard to distinguish the change. This difficulty has been reported in previous studies [27]. In the present experiment it was not possible to distinguish the solidus position accurately from the recorded video after 3500 s. The illumination of the test cell was changed after this experiment to better facilitate the observation of the solidus interface.

3.4. Solution at 6 wt%

The eutectic transformation occurs at a liquid fraction of 30% for an ammonium chloride solution of initial concentration of 6 wt%. This is significantly higher than the value of 55 for a 1 wt% solution. Experiments were conducted for a solution of this concentration.

The effect of the dissolved air in the liquid can be assessed by comparing the transient dimensionless temperature distributions for experiments with degassed and saturated solutions shown in Fig. 9. Essentially, the presence of a larger number of air bubbles in the mushy zone for experiment S06A has no effect on the temperature distributions. The temperatures measured by the thermocouples show an excellent agreement both in the liquid and mush regions. A small fluctuation in the temperature revealed by the first thermocouple can be observed for about 250 s into the experiment, and it is due to a failure in the booster pump, which was promptly fixed.

The liquidus and solidus interface positions may also be compared for examining the effect of the dissolved gas in the liquid. Figure 10 presents the interface positions with time. The liquidus and solidus interface positions for both experiments agree well. There is greater scatter of the data in the solidus than in the liquidus region, because of the difficulties associated with its observation, but this is within the experimental uncertainty. The liquid fraction of the mushy region at the solidus interface is equal to 30%, which is still a small value.

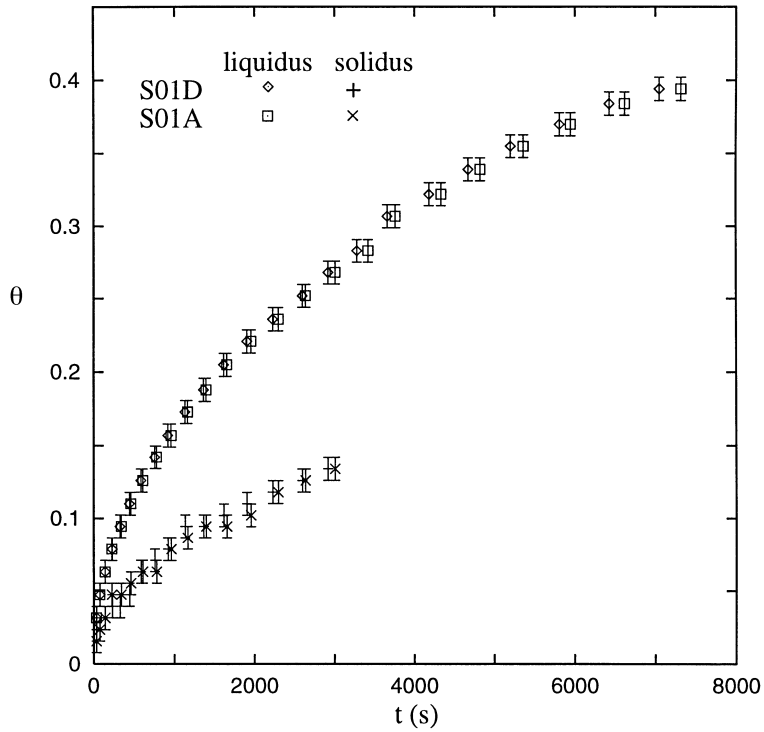

Fig. 8. Comparison of the liquidus position for experiments S01D and S01A.

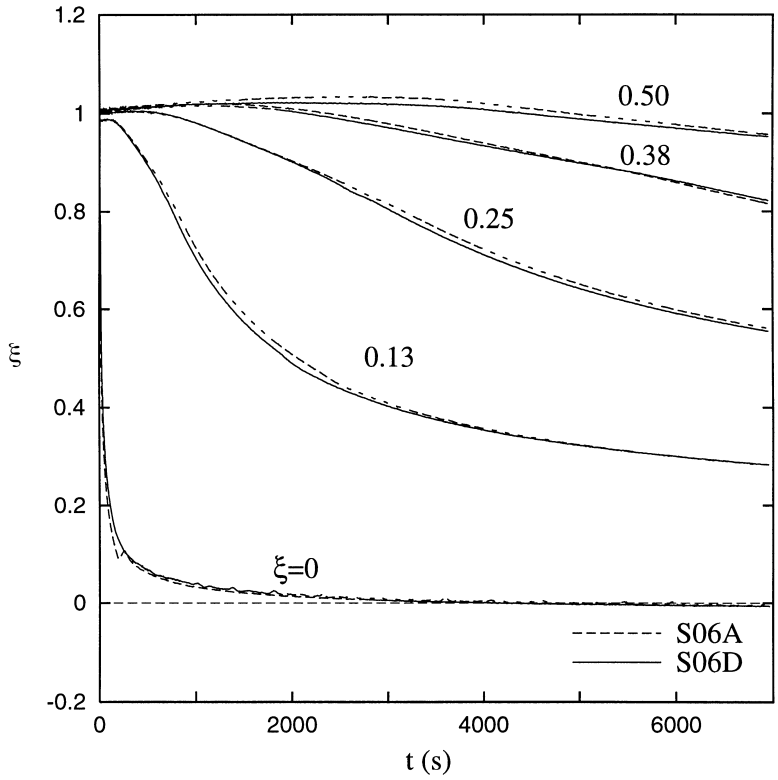

Fig. 9. Transient dimensionless temperature distribution of experiments S06D and S06A.

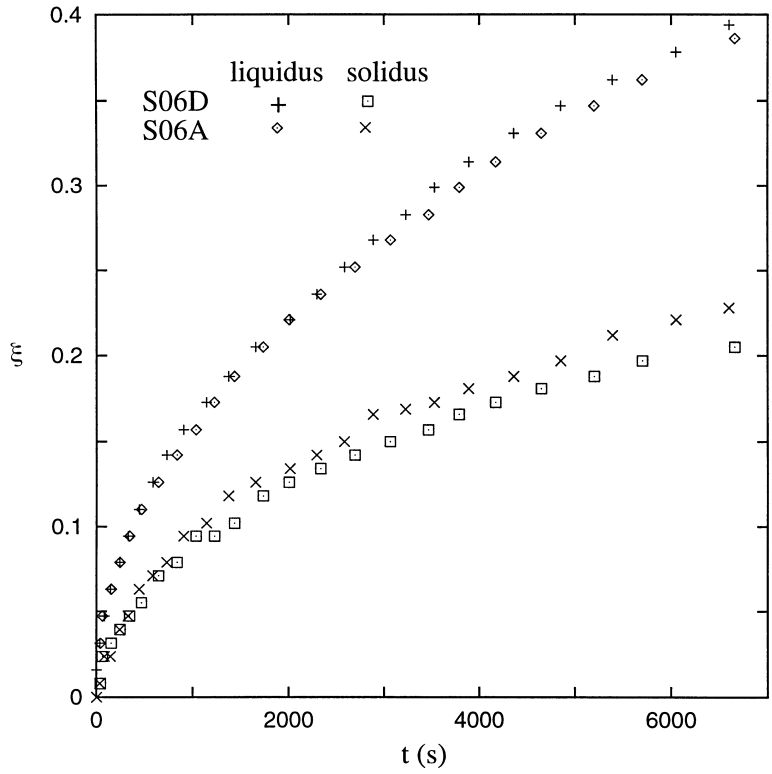

Fig. 10. Solidus and liquidus interface positions with time for experiments S06D and S06A.

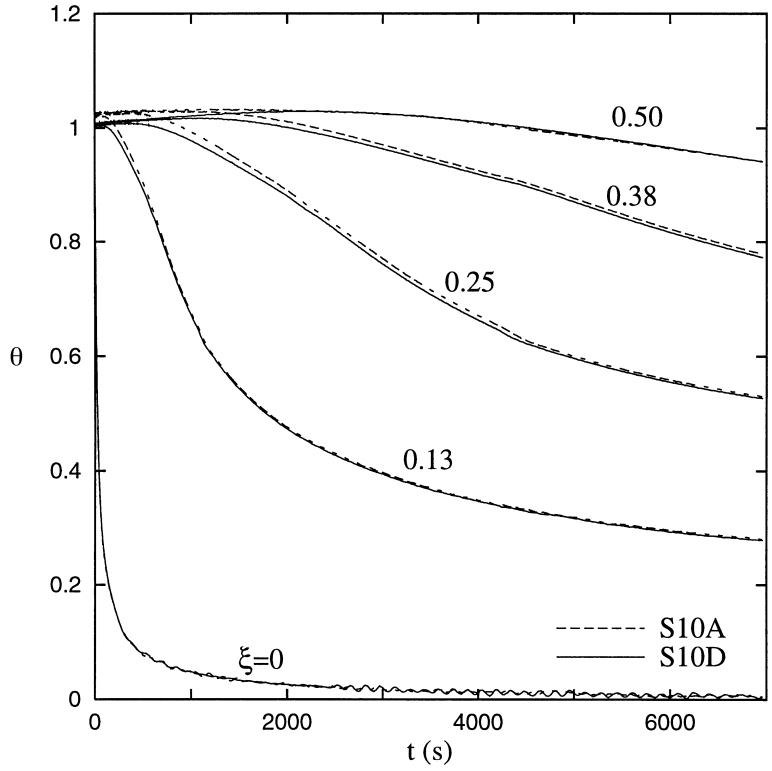

Fig. 11. Transient dimensionless temperature distribution of experiments S10D and S10A.

3.5. Solution at 10 wt%

For a solution with an initial salt concentration of 10 wt% the liquidus temperature is $-7°C$, and the liquid fraction prior to the eutectic transformation is 50.8%. As for the two previous concentrations (1 and 10 wt%), the experiments were conducted at a higher and a lower initial temperature and for two distinct amounts of air dissolved in the liquid.

The transient dimensionless temperature distribution for Experiments S10D and S10A are shown in Fig. 11. As for the two previous initial concentrations, the temperatures show an excellent agreement, leading to the conclusion that the air dissolved in the liquid does not play an important role in the heat diffusion process. The temperature measured by the first thermocouple ($\xi = 0$) for Experiment S10D reveals an oscillation of less than 0.5°C due to the controller of the constant temperature bath.

Figure 12 presents the interface positions with time for experiments S10D and S10A. The liquidus and solidus interface position for both experiments agree very well. Note that the solidus interface positions increases monotonically with time and is smoother. This is due to the greater contrast between the mushy and the completely solidified region, since the liquid fraction of the mushy region at the solidus interface is much larger for this than for both previous initial salt concentrations. Note that the region with solid crystals is smaller and that the mushy zone is thinner than the one for the two lower concentrations.

4. Conclusions

Solidification of water and an aqueous ammonium chloride solution was studied within a rectangular test cavity, which was cooled and heated at top and bottom walls by imposing uniform but different temperatures. The transport of heat and species during the solidification experiments was controlled by diffusion, since the conditions of the experiments were chosen to avoid buoyancy driven flow. Temperature and interface positions were measured for water and for four solutions of different initial NH_4Cl concentration. The amount of dissolved air in the liquid was controlled by imposing the ambient pressure around the test cell. The following conclusions can be drawn:

(1) Water was solidified from above with an initial temperature lower than 3.98°C to avoid buoyancy driven flow generated by density inversion. Three different amounts of dissolved air were studied: saturated at 1 atm, degassed, and supersaturated at a low pressure.

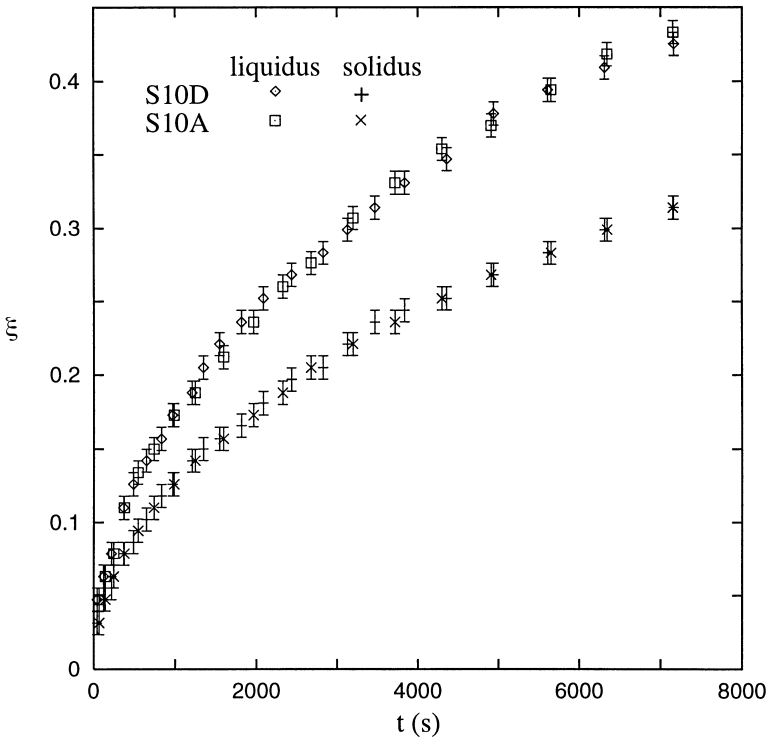

Fig. 12. Solidus and liquidus interface positions with time for experiment S10D and S10A.

The temperature distribution and the solid–liquid interface position did not indicate significant differences due to the presence of dissolved air.

(2) The air dissolved in the liquid did not affect the propagation of the interfaces or the temperature distribution for the aqueous solutions of NH_4Cl studied, leading to the conclusion that gas evolution and bubble nucleation in the interdendritic region does not significantly affect the transport of heat and species during solidification.

Hence, we conclude that the results of previous solidification experiments, where the phase change material was water or a salt solution with a moderate solidification rate (which is the case for most of the previous work using salt solutions) were not affected by the dissolved air in the liquid. This is the case even when the liquid was not degassed.

Acknowledgement

Marcus V. A. Bianchi gratefully acknowledges support of his doctoral studies by the Conselho Nacional de Desenvolvimento Científico e Tecnológico (CNPq—Brazil).

References

[1] W. Kurz, D.J. Fisher. Fundamentals of Solidification, 3rd ed., Chap. 1, Trans Tech Publications, Aedermannsdorf, Switzerland, 1989.

[2] R. Viskanta, Phase change heat transfer, in: G.A. Lane (Ed.), Solar Heat Storage: Latent Heat Materials, Chap. 5, CRC Press, Boca Raton, FL, 1983.

[3] J.O.M. Karlsson, M. Toner, Long-term storage of tissues by cryopreservation: critical issues, Biomaterials 17 (1996) 243–256.

[4] S.M. Copley, A.F. Giamei, S.M. Johnson, M.F. Hornbecker. The origin of freckles in unidirectionally solidified castings, Metallurgical Transactions 1 (1970) 2193–2204.

[5] A.F. Giamei, B.H. Kear. On the nature of freckles in nickel base superalloys, Metallurgical Transactions 1 (1970) 2185–2192.

[6] S. Asai, I. Muchi, Theoretical analysis and model experiments on the formation mechanism of channel-type segregation, Transactions ISIJ 18 (1978) 90–98.

[7] T.D. McCay, M.H. McCay, S.A. Lowry, L.M. Smith, Convective instabilities during directional solidification, Journal of Thermophysics and Heat Transfer 3 (1989) 345–350.

[8] D.G. Neilson, F.P. Incropera, Unidirectional solidification of a binary alloy and the effects of induced fluid motion, International Journal of Heat and Mass Transfer 34 (1991) 1717–1732.

[9] C.S. Magirl, F.P. Incropera, Flow and morphological conditions associated with unidirectional solidification of aqueous ammonium chloride, ASEM Journal of Heat Transfer 115 (1993) 1036–1043.

[10] M. Song, Solidification of an anisotropic porous medium saturated with a binary alloy, Ph.D. thesis, Purdue University, West Lafayette, IN, 1995.

[11] V.J. Colangelo, F.A. Heiser, Analysis of Metallurgical Failures, 2nd ed., Chap. 11, John Wiley & Sons, New York, 1987.

[12] L.W. Eastwood, Gas in Light Alloys, Chap. 1, John Wiley & Sons, New York, 1946.

[13] W.R. Wilcox, V.H.S. Kuo, Gas bubble nucleation during crystallization, Journal of Crystal Growth 19 (1973) 221–228.

[14] K.F. Vasconcellos, J. Beech, The development of blowholes in the ice/water/carbon dioxide system, Journal of Crystal Growth 28 (1975) 85–92.

[15] K. Tagavi, L.C. Chow, K.A. Tagavi, Void formation in unidirectional solidification, Experimental Heat Transfer 3 (1990) 239–255.

[16] C.D. Sulfredge, L.C. Chow, O. Solaiappan, Solidification void formation for cylindrical geometries, Experimental Heat Transfer 3 (1990) 257–268.

[17] M.V.A. Bianchi, R. Viskanta, Gas segregation during solidification processes, International Journal of Heat and Mass Transfer 40 (1997) 2035–2043.

[18] M.V.A. Bianchi, Crystal morphology and gas evolution during solidification processes, Ph.D. thesis, Purdue University, West Lafayette, IN, 1997.

[19] B. Gebhart, U. Jaluria, R.L. Mahajan, B. Sammakia. Buoyancy-Induced Flows and Transport, Hemisphere, Washington, DC, 1988.

[20] F.P. Incropera, D.P. DeWitt. Fundamentals of Heat and Mass Transfer, 4th ed., John Wiley & Sons, New York, 1996.

[21] R. Cohen-Adad, J.W. Lorimer (Eds.), IUPAC Solubility Data Series—Alkali Metal and Ammonium Chlorides in Water and Heavy Water (Binary Systems), Pergamon Press, New York, 1991.

[22] R. Bennacer, L.Y. Sun, Y. Toguyeni, D. Gobin, C. Benard. Structure d'écoulement et transfert de chaleur par convection naturelle au voisinage du maximum de densité, International Journal of Heat and Mass Transfer 36 (1993) 3329–3342.

[23] D. Gobin, R. Bennacer. Double diffusive natural convection in aqueous solutions near the density maximum, International Communications in Heat and Mass Transfer 23 (1996) 971–982.

[24] I.D. Zaytsev, G.G. Aseyev (Eds.), Properties of Aqueous Solutions of Electrolytes, CRC Press, Boca Raton, 1992.

[25] E.W. Washburn (Ed.), International Critical Tables of Numerical Data, Physics, Chemistry and Technology, McGraw-Hill, New York, 1928.

[26] S.L. Braga, R. Viskanta, Solidification of a binary solution on a cold isothermal surface, International Journal of Heat and Mass Transfer 33 (1990) 745–754.

[27] D.G. Neilson, Unidirectional solidification of a binary alloy and the effects of induced fluid motion, Ph.D. thesis, Purdue University, West Lafayette, IN, 1991.